J Solid State Electrochem (2012) 16:3515–3528
DOI 10.1007/s10008-012-1870-9

ORIGINAL PAPER

Electrochemistry of MoO_3–K_2MoO_4 melts: a chance to control the nature of reduced molybdenum oxides

Veronika K. Laurinavichyute · Sergey Yu. Vassiliev · Alexander Yu. Filatov · Eduard E. Levin · Galina A. Tsirlina

Received: 2 May 2012 / Revised: 5 September 2012 / Accepted: 6 September 2012 / Published online: 26 September 2012

Abstract Cathodic electrodeposition of oxides on platinum from MoO_3–K_2MoO_4 (3.85–75 mol% MoO_3) under DC and pulsed galvanostatic modes is discussed in combination with voltammetry data. Characteristic potential values (as related to oxygen evolution onset) are reported for Mo(VI/IV) redox processes, as well as for electrochemical equilibria with participation of molybdenum metal and Pt–Mo alloys. On the basis of scan rate effects and results for various potential limits, and also of voltammetry with preliminary potentiostatic accumulation of products, molybdate reduction mechanism complicated by a chemical step of Mo metal oxidation is proposed. This qualitative assumption is verified in preparative electrolysis experiments with products identification by means of X-ray diffractometry, scanning electron microscopy, and EDX local analysis. Deposition under pulsed mode is found to be useful tool to adjust the duration of chemical step and by these means to alter the composition of final products. The conditions supporting the formation of MoO_2 and more reduced oxides are formulated.

Keywords Molybdenum reduced oxides · Electrochemical–chemical mechanism · Pulsed deposition

Electronic supplementary material The online version of this article (doi:10.1007/s10008-012-1870-9) contains supplementary material, which is available to authorized users.

Dedicated to Professor Waldfried Plieth, the unique expert on electrodeposition of complex solids.

V. K. Laurinavichyute (✉) · S. Y. Vassiliev · A. Y. Filatov · E. E. Levin · G. A. Tsirlina
Department of Chemistry, M.V. Lomonosov Moscow State University,
119991, Moscow, Russian Federation
e-mail: nika@elch.chem.msu.ru

Introduction

Basic M_2MoO_4–MoO_3 melts (where M=Li, Na, K, Rb) with the addition of various oxides are widely used in electrosynthesis of compounds with strong metal–metal interactions, either in the form of clusters or as extended metal–metal bonded chains. Representative examples are KMo_4O_6 [1], $La_5Mo_4O_{16}$ [2, 3], $LaMo_{8-x}O_{14}$ [4], $NdMo_6O_{12}$ [5], or $Sm_4Mo_{18}O_{32}$ and $Nd_4Mo_{18}O_{32}$ [6]. These syntheses require high temperatures (T=1,200–1,300 K) and low acidity of the melt (typically ca. 14–35 mol% MoO_3; melt acidity can be also varied by rare earth oxides additives).

Molybdenum bronzes can be deposited from more acidic molybdenum melts (75–79 mol% MoO_3) with lower melting temperatures (T_m) [7–13] if superheat does not exceed 25 °. Moreover, even in this narrow interval one can obtain different bronzes depending on the deposition temperature ($K_{0.3}MoO_3$ at 823 K or $K_{0.33}MoO_3$ at 833 K, [7]) using similar current densities. At higher temperatures, MoO_2 forms exclusively, probably due to thermal decomposition of bronzes. Similar trends are known for lithium bronzes [12], but in this case crystals form in the melt bulk, not at the electrode surface (perhaps because of bronze high solubility in the melt). One of the factors affecting the structure of electrodeposited oxides can be the existence of certain ionic species (e.g., $(Mo_6O_{22})^{8-}$ [14, 15]) serving as precursors.

Despite wide applications of M_2MoO_4–MoO_3 melts in electrosynthesis, the mechanisms of corresponding electrode processes as a whole were never discussed. Moreover, rather limited information is available on electrochemical equilibria and kinetics of electrode processes in these [16, 17] or similar oxide and oxide–halide [18, 19] melts. Furthermore, experimental details of the reported electrosyntheses are usually incomplete (e.g., current density is often omitted). Electrosyntheses using such melts were conducted

under galvanostatic mode, and three-electrode configuration of the cell has never been reported, so that it is impossible to assign deposition processes to potentials investigated. To choose the proper electrodeposition conditions for particular reduced molybdenum oxide, this information is of crucial importance.

The aim of the present work is to systematically investigate the electrochemical behavior of high- and low-temperature oxomolybdenum melts. We would like to check the role of various factors on current response in the certain potential regions. Unfortunately, in contrast to solution electrochemistry, it is difficult to vary the temperature and composition of the melt independently. Our efforts are aimed to arrange electrodeposition of various reduced molybdenum oxides under more precise electrochemical and compositional control.

Experimental

Preparation of the electrolyte

Melts with various MoO_3 molar contents (3.85–75 mol%) were prepared either by mixing the proper amounts of MoO_3 and K_2CO_3, or by adding the required quantities of MoO_3 to the melt of known composition. Prior to mixing, all reagents were subjected to preliminary heat treatment for 48 h at 773 K in air. All reagents were of pure-grade quality. The mixture (50–75 g) was melted in high-density alumina crucible. All experiments were carried out in air. Melt temperature was monitored using IR pyrometer "Kelvin". Independent temperature control for low-temperature melts was performed using glass-covered chromel–alumel thermocouple immersed directly in the melt.

The following series of melts were studied.

1. Constant acidity (50 mol% MoO_3) series at varied temperature (823–933 K).
2. Constant temperature (1,233 K) series at varied acidity (3.85–50 mol% MoO_3).

Some impurities in the melt are unavoidable due to slow dissolution of the crucible material and occasional crumbling of thermal protection elements. The traces of these impurities (typical for high-temperature melt electrochemistry), namely of Al, Ti, and Si, were found in some deposits under study. Fortunately, Al and Si never interplay with Mo in oxide lattices. As for Ti, to check its ability for Mo substitution we arranged several test depositions from the melts with different TiO_2 additives. It was found that depending on TiO_2 content titanium-substituted KMo_4O_6 or hollandite can be obtained. Detailed discussion of the obtained substituted structure will be published elsewhere. We have never observed these compounds in our experiments without TiO_2 addition, but we cannot exclude formation of other slightly substituted KMo_4O_6 in this case.

Electrochemical apparatus

All electrochemical experiments were performed using potentiostat Autolab PGSTAT30. For pulsed electrodeposition, additional ac-component was imposed by PC Function Generator Velleman PCG 10/8016 (+PC scope Velleman PCS500).

Platinum wires of 0.5 mm diameter were used as working and quasi-reference electrodes in cyclic voltammetry experiments. The immersion depth 10±1 mm of the working electrode was fixed by controlled movement of the electrode in vertical direction after the establishment of electrical contact with the melt. Correspondingly, the geometric area was 0.16±0.02 cm^2. The potential of the quasi-reference electrode is determined mostly by oxygen-related equilibria. Its behavior is dependent on the surface state, i.e., on the presence of platinum oxide films and their thickness (which changes unavoidably in the course of measurements). To increase the accuracy, all measured potentials were corrected with respect to onset of anodic process demonstrating a sharp current growth. The latter was associated with oxygen evolution, as thermodynamics predicts no other anodic reactions in the system under study. Typically the potential of Pt quasi-reference was about 0.1–0.15 V more negative than the onset of oxygen evolution.

The onset potential of oxygen evolution was estimated from extrapolation of the initial linear segment of oxygen evolution I, E curve to zero current. All potentials are given below versus this O_2 evolution potential. A typical error of potential values determination can be estimated as ±10 mV. All current densities presented below are normalized per immersed geometric area of the working electrode. The counter electrode was a 2.5-cm^2 platinum slab. Ohmic drops (typically 1.3–5 Ohm) were estimated from high frequency (ca. 10 kHz) impedance values and partly compensated (75–85 %) in all voltammetric experiments. All presented CVs are stabilized (it is possible after three to five cycles). CVs are reproducible in independent experiments for one and the same melt composition/temperature, excluding very few features specially mentioned in the text.

Preparative electrodeposition

Preparative electrodeposition experiments were performed either in three-electrode (with quasi-reference) or two-electrode cell. Working and counter electrodes were 2.5–4.0 cm^2 platinum slabs (with platinum wire connectors) completely immersed in the melt. For preparative electrodeposition, we used galvanostatic mode or applied cathodic square wave pulses (−0.1 $A cm^{-2}$/open circuit, frequency

(f)=3 Hz). During pulsed deposition the duration of cathodic current (duty cycle) was varied from 33 to 67 % of the total pulse time.

Melt quantity was generally enough to avoid the pronounced changes of bulk composition in the course of long-term experiments. Some changes (and corresponding shifts of quasi-reference potential) were only observed in the melts with very low MoO_3 content.

After electrolysis all electrodes with deposits and remaining melt were successively sonicated in hot solution of 2 M HCl and distilled water using "Saphir" (UZV-1,3) ultrasonic bath. Typically, the precipitates were easily separated from electrodes. After washing, precipitates were separated from solution by decantation with or without prior centrifugation. The bright blue color of the washing solution indicates partial dissolution of some reduced molybdates, which results in underestimation of current efficiency. After spending the charge of 1,400 $C\,cm^{-2}$ under either galvanostatic or pulsed mode, the typical deposit mass recovered after washing was 0.2–0.3 $g\,cm^{-2}$. Thus estimated current efficiency only rarely exceeded 3–4 % for reduction of MoO_3 to KMo_4O_6. The highest observed current efficiency was 6 %. The estimated loss of the deposit (from visual observations after washing) does not exceed a half of initially formed quantity, so real current efficiency is in any case below 10 %. The majority of charge is spent for formation of reduced molybdates soluble in the melt.

After certain experiments, especially in high-temperature melts, platinum cathode appeared to be covered with dark and highly adhesive film, which could be removed only by prolonged boiling in aqua regia or firing with NaOH in hydrogen flame. The nature of this film remains unknown and requires further study.

Characterization

X-ray powder diffraction data were collected at room temperature using Huber G670 Image Plate Guinier camera (Cu $K\alpha_1$ radiation) and a θ–2θ Bragg–Brentano RIGAKU D/max RC diffractometer (Cu Kα radiation) equipped with a secondary graphite monochromator and a scintillation counter. Phase identification was performed using ICDD PDF-2 [20] database and FIZ/NIST ICSD [21] databases. For quantitative phase analysis, the derivative difference minimization (DDM) routine [22] was used as implemented into DDM 1.93 software package [21].

Only major phases belonging to K–Mo–O system are pointed out. In fact, in all obtained diffraction patterns of deposits some weak (relative intensity less than 5 %) unidentified diffraction peaks were observed, so the data given below should be treated as the relative content of identified phases. Unknown phases can result from contaminations (deposit interaction with crucible and/or electrode materials).

Chemical compositions of bulk samples were analyzed by energy-dispersive X-ray spectroscopy (EDX) with JEOL JSM6490 LV scanning electron microscope (LaB_6 cathode, 20 kV) equipped with EDS spectrometer INCA X-Sight (Oxford Instruments). EDX measurements were performed with standard-free method at five to seven points for each type of crystal in certain sample.

Results and discussion

Thermodynamic estimates

To assign electrochemical responses to certain processes, we used preliminary estimates based on HSC thermodynamic data for solids and oxygen [23]. Table 1 collects Gibbs energies for various chemical redox processes and corresponding standard potentials for half-reaction equilibria[1] with participation of different molybdenum-based redox systems. The latter values are given in relation to oxide/O_2 potential[2]; this scale is used below and denoted as 'vs. O_2'. Standard potentials for redox systems associated with possible impurities are listed as well. As can be seen from Table 1, impurities reduction (Al_2O_3, SiO_2, and TiO_2) can start only at more negative potentials as compared to Mo (VI) and Mo(IV) reduction to Mo metal. Minor overlap of redox responses can be expected only for reduced titanium oxides formation (e.g., Ti_nO_{2n-1}) at high temperatures, but as concentration of Ti species is much lower than of Mo species, this can hardly provide any noticeable contribution to current values.

It is worth noting that experimentally estimated equilibrium potential values may differ from calculated standard values not only due to concentration factor but also due to different state of molybdenum-containing species in solids and in the melt. Namely, solvation, ionic association, oxomolybdate polycondensation, dipole–dipole, or any other interactions in the melt affect this state and can be formally taken into account in terms of activity coefficients. No experimental data on activities in the K_2MoO_4–MoO_3 melts can be found in the literature, so more precise equilibrium potentials cannot be calculated for this system. For Na_2O–MoO_3 melts with 50.9–92.2 mol% MoO_3, the activities are available for 890–1,230 K temperature interval [24]. Extrapolation of these data to basic melts (3.85 mol% MoO_3) results in cathodic shift of the calculated standard potentials to −0.46 V for MoO_3/MoO_2 and to −0.15 V for MoO_3/Mo.

[1] We use term "standard", despite of non-ambient temperature, because these values correspond to activities of all dissolved components equal to unity.

[2] Our experimental approach to attribute potentials to this scale using the onset of oxygen evolution can result in ca. 5–10 mV shift, which is within typical accuracy of potential measurement.

Table 1 Thermodynamic estimates of Gibbs energies and standard potentials $E°$ (vs. O_2) for various redox-processes at 843 and 1,233 K on the basis of free energy data for solids and oxygen [23]

Reaction	843 K		1,233 K	
	ΔG_{843}, kJmol^{-1}	$E°$, V	$\Delta G_{1,233}$, kJmol^{-1}	$E°$, V
$K_2MoO_4=K_2O+Mo+1.5O_2$	877.6	−1.516	694.3	−1.20
$2K_2O=4\ K+O_2$	486.9	−1.261	399.6	−1.035
$2K_2MoO_4=2MoO_2+2K_2O+O_2$	885.7	−2.294	652.9	−1.691
$MoO_3=Mo+1.5O_2$	530.9	−0.917	445.6	−0.770
$2MoO_3=Mo+MoO_2+2O_2$	627.0	−0.812	523.3	−0.678
$2MoO_3=2MoO_2+O_2$	192.3	−0.498	155.4	−0.403
$Mo+2MoO_3=3MoO_2$	−242.5		−212.4	
$MoO_2=Mo+O_2$	434.8	−1.126	367.9	−0.953
$8MoO_3=8MoO_{2.75}+O_2$	171.7	−0.445	179.4	−0.465
$16MoO_3=16MoO_{2.875}+O_2$	161.0	−0.417	226.6	−0.587
$18.018MoO_3=18.018MoO_{2.889}+O_2$	159.7	−0.414	240.1	−0.622
$TiO_2=Ti+O_2$	790.5	−2.048	721.4	−1.869
$8TiO_2=2Ti_4O_7+O_2$	576.9	−1.495	491.9	−1.274
$6TiO_2=2Ti_3O_5+O_2$	588.6	−1.525	501.7	−1.300
$4TiO_2=2Ti_2O_3+O_2$	597.0	−1.547	523.5	−1.356
$SiO_2=Si+O_2$	757.8	−1.963	690.0	−1.788
$Al_2O_3=2Al+1.5O_2$	1,411.2	−2.438	1,283.7	−2.217

Nevertheless, one can assume better agreement of calculated and experimental characteristic potentials of MoO_3/Mo and MoO_3/MoO_2 pairs in acidic melts, when activity is close to unity.

We should also mention another complication: if Mo–Pt alloy is formed instead of Mo metal, equilibrium potentials can also shift with respect to calculated values. Taking into account the available enthalpies of formation of Mo–Pt alloys ($\Delta_f H°(MoPt)=-26.1$ kJmol^{-1}, $\Delta_f H°(MoPt_2)=-36.9$ kJmol^{-1} [25]) and neglecting unknown entropy contributions, one can expect the potential shift up to $0.270/n$–$0.380/n$ V for n-electron equilibria. Thus, the highest possible anodic potential shift for redox process Mo/MoO_3, as induced by alloy formation, is about 0.045–0.065 V. Similar result (ca. 0.05 V shift) can be obtained with typical standard Gibbs energies of formation for platinum-rich intermetallic compounds (5–25 kJmol^{-1} at 1,233 K [26]).

Keeping in mind these thermodynamic circumstances, one can expect the formation of reduced molybdenum oxides with formal oxidation state of Mo above IV at relatively high potentials (> −0.4 V). Another important prediction from Table 1 is the thermodynamic instability of metallic molybdenum at high temperatures in presence of oxygen, as can be seen from the negative values of ΔG for oxidation reactions (Mo/MoO_2, Mo/MoO_3).

Determination of equilibrium potentials from experimental data in the melts presents a challenge since the majority of electrochemical responses are less reversible or completely irreversible. In what follows, the efforts were concentrated on the assignment of observed voltammetric features to certain redox pairs. The goal was to collect potentials of various pairs and to specify thermodynamic predictions for formation of certain products. Basically, three types of redox behavior were observed in cyclic voltammograms (CVs), which are illustrated in Figs. 1, 2, 3 and 4.

(a) A sharp increase of both anodic and cathodic currents in the vicinity of a characteristic potential. In this case characteristic potential value can be determined as the potential of zero current (e.g., E/E', G/G' in Fig. 4), and it is expected to be close to equilibrium potential.

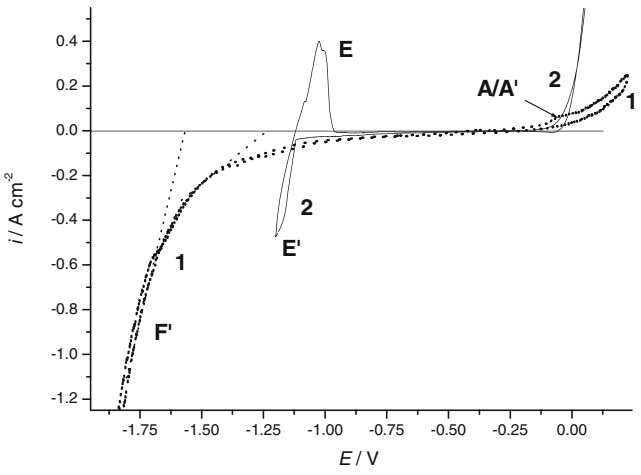

Fig. 1 Cyclic voltammograms of platinum electrode in pure K_2MoO_4 (*1*) and K_2MoO_4 with 3.85 mol% MoO_3 (*2*) melts. Scan rate 100 mV s^{-1}. T=1,233 K. *Dashed slight lines* demonstrate the estimates of characteristic potentials according to procedure (b), see text for details

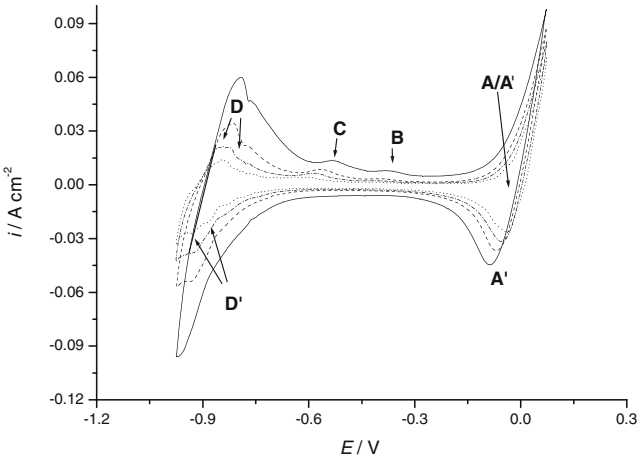

Fig. 2 Cyclic voltammograms of platinum electrode in 75 mol% K_2MoO_4–25 mol% MoO_3 melt. Scan rates 2.5, 5, 10, and 25 Vs^{-1}, T=1,073 K

(b) Completely irreversible reduction/oxidation. In this case, characteristic potential could be determined only by extrapolation of the initial segment of I, E curve to zero current (B, C, F', G', e.g., in Figs. 1, 2, and 3).[3] Correspondingly, a deviation from equilibrium potential could be rather high. Nevertheless, a characteristic potential is helpful to predict the formation of certain products.

(c) Quasi-reversible behavior. This gives a chance to determine characteristic potential as a half sum of peak potentials (A/A', C/C', D/D', e.g., in Figs. 2 and 3a); thus determined value are close to equilibrium potential.

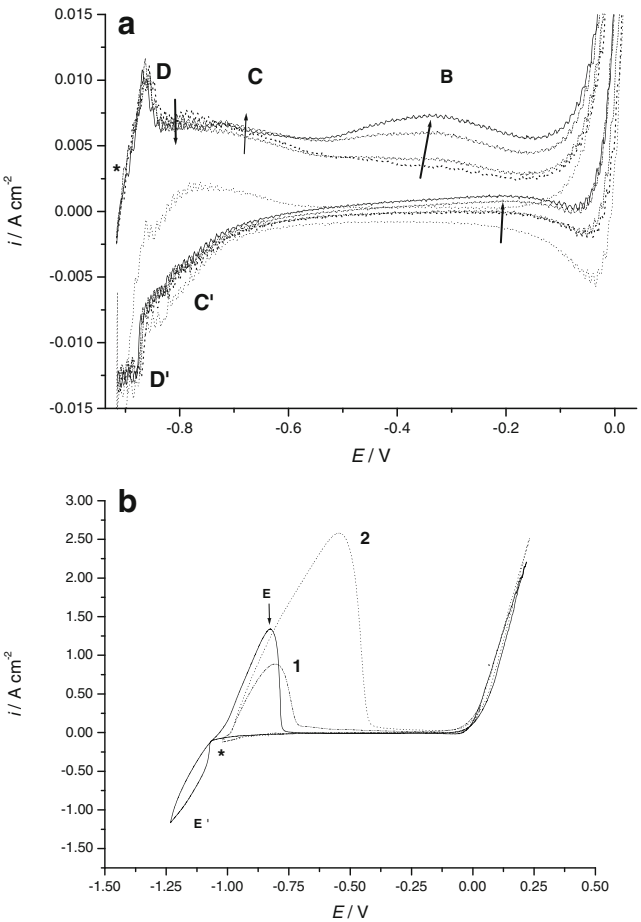

Fig. 3 Cyclic voltammograms of platinum electrode in K_2MoO_4 with 14.3 (**a**) and 20 (**b**) mol% MoO_3 melts after electrode pretreatment for 1–15 min at −0.915 V (**a**) or for 1 (*1*) and 3 min (*2*) at −1.030 V (**b**). Scan rate 100 mVs^{-1}, T=1,233 K. *Asterisk* shows accumulation potential. *Thick arrows* demonstrate the trend

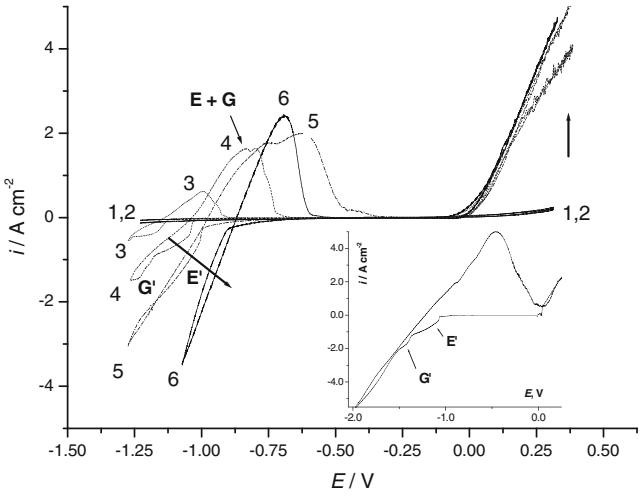

Fig. 4 Cyclic voltammograms of platinum electrode in K_2MoO_4–MoO_3 melts with various MoO_3 contents (mol%): 0 (*1*), 3.85 (*2*), 16.7 (*3*), 25 (*4*), 40 (*5*), and 50 (*6*). *Inset* presents cyclic voltammogram (*5*) in a wider potential range scan rate 100 mVs^{-1}, T=1,233 K

The error of all characteristic potentials determination can be estimated as ±15 mV.

High-temperature melts (1,233 K)

Typical CV of platinum electrode in molten K_2MoO_4 (curve 1, Fig. 1) demonstrates that irreversible cathodic process starts at ca. −1.2 V. Sharper current increase with negative potential can be noticed starting from ca. −1.6 V. According to thermodynamic data (Table 1), this process can be attributed to K_2MoO_4 reduction with formation of Mo (E=−1.20 V)[4]. Additional current increase can be assigned to reduction of K_2O (see standard potential in Table 1). Redox process A/A' in the vicinity of 0 V (see also in Fig. 2) overlaps with oxygen evolution and can be assigned to platinum oxidation/reduction.

[3] Processes G/G', C/C', and B/B' demonstrate different types of redox behavior in the melts of various composition that is why corresponding characteristic potentials were determined via different procedures.

[4] Here and below standard potentials from Table 1 are recalculated for certain concentration or (if available) activity.

MoO_3 addition (curve 2, Fig. 1) results in significant increase of anodic current corresponding to oxygen evolution and Pt oxides formation (Fig. 2, peaks *A*, *A′*). Simultaneously, a new feature at ca. −1.15 V appears. In addition, several minor peaks can be marked out, but only when scanning narrower potential region with much higher scan rates (*v*) and in the melts with higher MoO_3 concentration (Fig. 2).

- Oxidation peak *B* (−0.38 V, 50 mol% MoO_3) is poorly reproducible. It can be detected without preliminary accumulation of reduced product only if MoO_3 content exceeds 25 mol%. In some melts, corresponding cathodic peak at ca. −0.42 V is also observed. Taking into account thermodynamic estimates, one can formally assume MoO_3/MoO_2 redox process. However, further experiments demonstrated that the electrodeposition of MoO_2 takes place at more negative potentials. Alternatively, this redox process can be ascribed to the oxidation of partially reduced oxomolybdate anions (absent from the available set of thermodynamic data).
- Another small anodic peak *C* at more negative potential (−0.64 V, 30 mol% MoO_3) and especially the corresponding cathodic peak (*C′*, observed only at high scan rates or after preliminary accumulation) are also poorly reproducible. The reliable assignment of *C*/*C′* couple requires additional experiments.
- Peaks *D*/*D′* at −0.97 and −0.92 V (3.85 mol% MoO_3) have a complex shape, but basically demonstrate the behavior typical for quasi-reversible process: the charges at anodic and cathodic scans are close, and peaks separation is ca. 25–30 mV (41 mV is expected for reversible process at 1,233 K). These peaks can be associated with oxidation/formation of either Pt–Mo solid solutions or intermetallic compounds ($MoPt_3$, $MoPt_2$, and MoPt are stable at 1,233 K [27]). Some evidence of Mo–Pt intermetallic compounds formation was also mentioned earlier by Topor et al. [28] who reported electrolysis of Li_2MoO_4 in LiF–NaF–KF melt at 873 K using platinum electrodes. Peak shapes can be attributed to the overlap of closely located peaks corresponding to subsequent steps of multielectron process.

One cannot exclude that minor peaks observed at high scan rates correspond to redox transformations of surface attached species (which can be treated as “double layer charging” in a wide sense). The charges corresponding to these peaks are comparable with “double layer” charges (but higher).

Useful information concerning reduction processes can be obtained from analysis of data for potentiostatic accumulation of the deposits. After polarization at potentials slightly (50 mV) more negative than the first reduction peak *D′* (see asterisk in Fig. 3a) and subsequent anodic scan, the broad anodic peak *B* appears at −0.31 V in the melt with 14.3 mol% MoO_3. The shift of preliminary polarization potential to more negative value induces the appearance of high and less reproducible peak (*E*) at the anodic scan, which disappears after further cycling. Example is shown for 20 mol% MoO_3, Fig. 3b. The featureless curve after two to three cycles coincides with horizontal part of CVs, the currents are below 0.1 $A cm^{-2}$ and cannot be seen in the scale of Fig. 3b. This anodic peak also appears in cyclic voltammograms at −1.09 V in basic melt (3.85 mol% MoO_3) and shifts towards more positive potentials with increase of MoO_3 content (Fig. 4). Corresponding reduction peak is poorly defined and strongly overlapped with the subsequent reduction process (*G′*), especially in basic melts. Thus, oxidation peak *E* surely has a complex nature.

In Fig. 5a, all characteristic potentials corresponding to observed processes are collected and compared with thermodynamic estimates, shown below the potential axes. Figure 5b combines all dependences of characteristic potentials on melt acidity, presented in terms of MoO_3 molar fraction ($N(MoO_3)$). It can be seen that the potentials of redox equilibria *C*/*C′*, *D*/*D′*, and *E*/*E′* depend strongly on MoO_3 content.

Namely, for *C*/*C′* the increase in MoO_3 content results in anodic shift of the potential with the slope of 200 mV per decade that corresponds to the transfer of approximately one electron ($n \sim 1$, weak reduction, one can assume the reduction of some polymolybdate anion). Linear dependence of peak *C* current vs. $v^{1/2}$ formally indicates mass transfer limitations of oxidation process in our laboratory cell. This means that the variable melt composition can be expected in the near-electrode diffusion layer.

Similar potential shift with melt acidity is observed for *D*/*D′* pair, which can be attributed to intermetallic compound formation. Scan rate diagnostics fails for this redox system because of strong overlap with other peaks at high and moderate scan rates.

The dependence of *E*/*E′* characteristic potential on $\log[N(MoO_3)]$ reveals two linear regions with the slopes ~50 and ~450 mV per decade (Fig. 5b), indicating different reduction processes in the melts with MoO_3 content below and above 20 mol%. This observation is in qualitative agreement with the data [18] reported for redox processes in Na_2WO_4–MoO_3 melt, but much lower concentration of MoO_3 corresponds to the bending point (4–5 mol% MoO_3). The authors of [18] attributed two observed regions in basic and acidic melts to redox processes $Mo_2O_7^{2-}$/Mo and $Mo_2O_7^{2-}$/MoO_2, respectively.

In the melts containing 20–50 mol% MoO_3 and at high temperatures, the major electrolysis product at the potentials

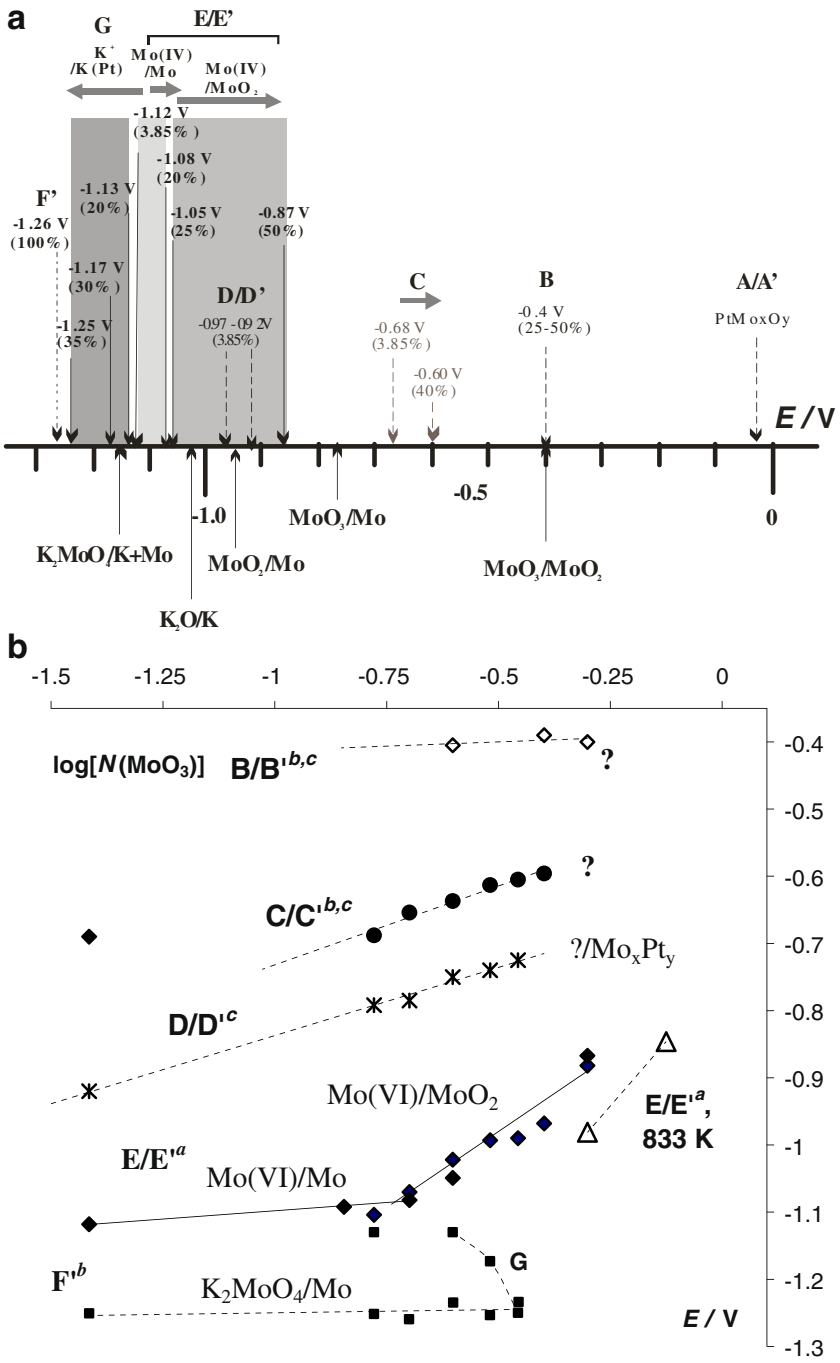

Fig. 5 Schematic representation of experimental characteristic potentials for different redox processes in K_2MoO_4–MoO_3 melt at 1,233 K (*above axes*), as compared with thermodynamic estimates (*below axes*). *Solid and dashed vertical arrows* indicate principal and weakly pronounced redox processes, respectively. Certain potentials and MoO_3 contents are given *near vertical arrows*. *Thick horizontal arrows* indicate the shift of characteristic potentials with melt acidity (increase of MoO_3 content). Like in Table 1, all thermodynamic estimates are given without regard to solvation, complex formation, or association (**a**). Effect of MoO_3 mole ratio on the experimental characteristic potentials for different redox processes in K_2MoO_4–MoO_3 melts at 1,233 K. For *E*/*E*′ process, points at 833 K are demonstrated as well (**b**). Assignment to certain redox pairs is given near each curve, "*?*" demonstrates the lack of assignment. *Superscripts a*, *b*, and *c* indicate determination procedure (see text)

of *E*′ region is MoO_2.[5] However, the *E*/*E*′ characteristic potentials are considerably more negative than thermodynamic estimates for MoO_3/MoO_2 reduction (−0.88 and −0.44 V, respectively, for the melt with 50 mol% MoO_3). This difference can be ascribed to the change of activity coefficients most likely caused by appearance of polymeric species (e.g., $Mo_2O_7^{2-}$, $Mo_3O_{10}^{2-}$, or $Mo_4O_{13}^{2-}$). Low number of electrons (n=0.5) formally estimated from the slope of *E*/*E*′ characteristic potential vs. log(N(MoO_3)) dependence does not contradict this hypothesis. Actually, it is very typical for polymolybdates when one electron per polyanion is transferred, which results in formal value below unity per Mo atom.

In basic melts (<20 mol% MoO_3), the reduction takes place at more negative potentials, and the dependence of formal potential on melt acidity is much weaker (n~5). The most natural hypothesis for the overall reaction is the reduction of MoO_3 to Mo.

[5] Minor change in melt composition due to overheating (160–460 °) cannot be excluded in these experiments.

The scan rate behavior of peaks E/E' is also unusual. When the scan rate is decreased, the second oxidation peak at more positive potential (−1.06 V) appears in basic melts (Fig. 6). Further decrease of scan rate results in redistribution of anodic peak heights. We assume that chemical oxidation of the previously deposited metallic molybdenum with formation of some product oxidizing at more positive potential is responsible for this behavior. For example, considering thermodynamic estimates one can expect chemical oxidation reactions $Mo+MoO_3=MoO_2$ or $Mo+O_2=MoO_2$. However, if being so, the appearance of the oxidation peak at −0.4 V should be expected. This contradiction can be eliminated if to assume that Mo metal undergoes oxidation to more reduced mixed valence oxide, like KMo_4O_6, at low MoO_3 content. Contrary, in the melts with higher MoO_3 molar fraction no redistribution in anodic peak heights was observed.

Characteristic potential of reduction process G' demonstrates a negative potential shift with melt acidity which can take place only for potassium ion reduction. At this stage, we can assume that reduction of potassium is possible at potentials less negative than estimated thermodynamic value because of K–Pt alloy formation.

As follows from this overview of redox processes, the voltammetric data can be self-consistently interpreted under assumption of chemical oxidation reaction proceeded by electrochemical reduction.

Preparative galvanostatic electrodeposition

When reduction takes place under diffusion limitations, the composition of near-electrode layer differs from bulk melt composition unavoidably.

Assuming electrochemical–chemical (EC) mechanism of MoO_3 reduction, one can suggest that molybdenum-to-oxide ratio in the near-electrode layer will define the molybdenum formal oxidation state in solid deposit as well as deposit phase composition. One should keep in mind that according to

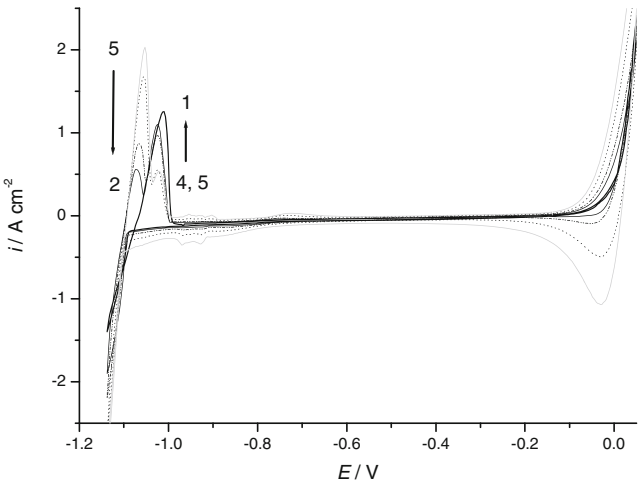

Fig. 6 Cyclic voltammograms of platinum electrode in 96.15 mol% K_2MoO_4–3.85 mol% MoO_3 melt. *Scan rates* 10 (*1*), 50 (*2*), 100 (*3*), 250 (*4*), and 500 (*5*)mVs^{-1}, T=1,233 K

Table 2 Electrodeposition conditions and the phase composition of products

Melt composition mol% MoO_3	i, A cm^{-2}	Temperature, K	Deposition time, h	Phase composition of deposit[c], wt%
3.85	−0.53	1,233[a]	5.0	Mo
	−0.18		19.5	KMo_4O_6—76±4 %
				Mo—20±1 %
				MoO_2—4±1 %
	−0.10		5.0	KMo_4O_6—85±3 %
				Mo—15±1 %
	−0.08		16.4	KMo_4O_6—99±4 %
				Mo—1±1 %
14.3	−0.06	1,233[a]	15.5	KMo_4O_6—96±1 %
				$K_3Mo_{14}O_{22}$—4±1 %
	−0.06		4.0	KMo_4O_6
20.0	−0.06	1,233[b]	13.75	KMo_4O_6—11±1 %
				MoO_2—89±2 %
	−0.25		1.5	KMo_4O_6—33±1 %
				MoO_2—67±3 %
25.0	−0.07	1,068[b]	2.0	MoO_2
	−0.24	1,233[b]	3.4	
	−0.06		4.6	
50.0	−0.05	823[b]	2.0	MoO_2
	−0.06	1,233[b]	18.4	MoO_2
75.0	−0.08	843[b]	1.25	$K_{0.3}MoO_3$—90±1 %
				$K_2Mo_4O_{13}$—5±1 %
				MoO_2—5±1 %
	−0.09	853[b]	1.0	$K_{0.3}MoO_3$—43±2 %
				$K_{0.33}MoO_3$—9±1 %
				$K_2Mo_4O_{13}$—48±2 %
Na_2MoO_4/ MoO_3 14.3	−0.15	1,213 C[b]	16.0	MoO_2
	−0.045	1,233[b]	10.75	MoO_2

[a] Formation of dark intermetallic compound on platinum surface was observed

[b] No darkening was observed

[c] KMo_4O_6 and $K_3Mo_{14}O_{22}$ were identified using the patterns calculated from crystal structure data [29] and [30]

thermodynamic data, MoO_3 itself can act as the oxidant at high temperatures. We performed a number of electrolyses with varied molybdenum-to-oxidant ratio by changing melt composition (MoO_3 content) or deposition current density (i.e., the rate of metallic Mo accumulation at the electrode surface; Table 2). XRD phase analysis confirmed that the increase in MoO_3 content results in changing the nature of deposition product from KMo_4O_6 to MoO_2. Low acidity of the melt and high deposition currents favor molybdenum metal formation as a major electrolysis product. The decrease of deposition current density induces the increase of KMo_4O_6 content in the mixture of Mo and MoO_2 (Fig. 7a). In both cases, typical electrode potential in the course of deposition was ca. −1.0–−1.1 V. At the same time, the formation of dark film on the cathode surface (perhaps intermetallic Pt–Mo compound) was detected. EDX data indicate the increase of Mo content in the film (Mo/K ratio of ca. 4.4) compared with its content in the melt as well as in KMo_4O_6 crystals (Mo/K~3.9). It can be seen from SEM image (Fig. 8) that KMo_4O_6 crystals growth takes place on top of this film at least at early stages. As already stated in the experimental part, although all the crystals can be easily detached from cathode surface in diluted HCl solution, the complete removal of the film can be achieved only after prolonged boiling in aqua regia.

Considering EC deposition mechanism even qualitatively, one can assume that it should affect significantly the microstructure of KMo_4O_6. There are three known modifications of KMo_4O_6: two orthorhombic forms KMo_4O_6-I and KMo_4O_6-II synthesized for the first time via solid-state reaction route [29] (KMo_4O_6-II being a high-pressure polymorph [29]), and one tetragonal form KMo_4O_6-III, which was earlier obtained by electrolysis [1]. According to XRD data, our crystals were identified as KMo_4O_6-III phase.

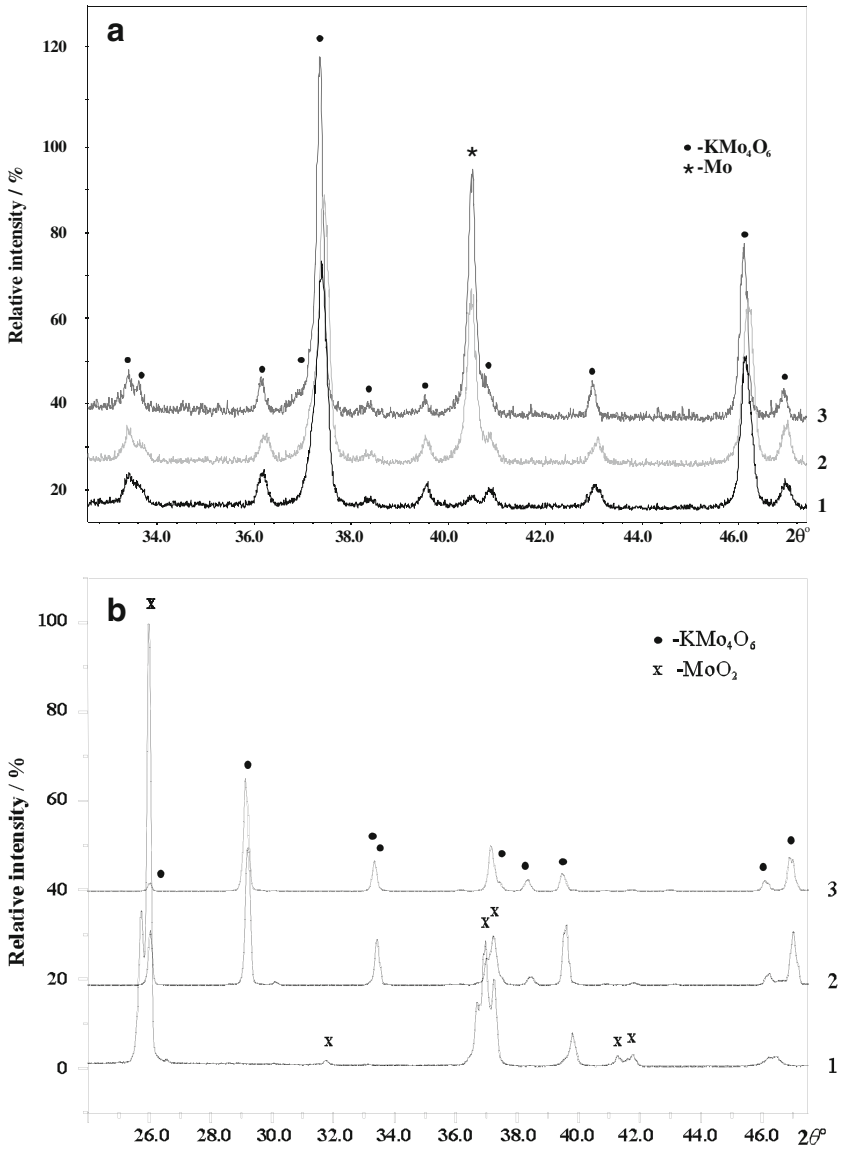

Fig. 7 The X-ray powder diffraction patterns of the electrodeposition products obtained in 96.15 mol% K_2MoO_4−3.85 mol% MoO_3 melt at current densities 0.08 (*1*), 0.1 (*2*), and 0.53 A cm^{-2} (*3*), T=1,233 K (**a**). The X-ray powder diffraction patterns of deposits obtained under pulsed regime in 85.7 mol% K_2MoO_4−14.3 mol% MoO_3 melt. Duty cycles: 23 % (*1*), 55 % (*2*), and 100 % (3), other conditions are the same as in Table 3 (**b**). T=1,233 K. The X-ray powder diffraction patterns for a wider angle range can be found in Supplementary materials

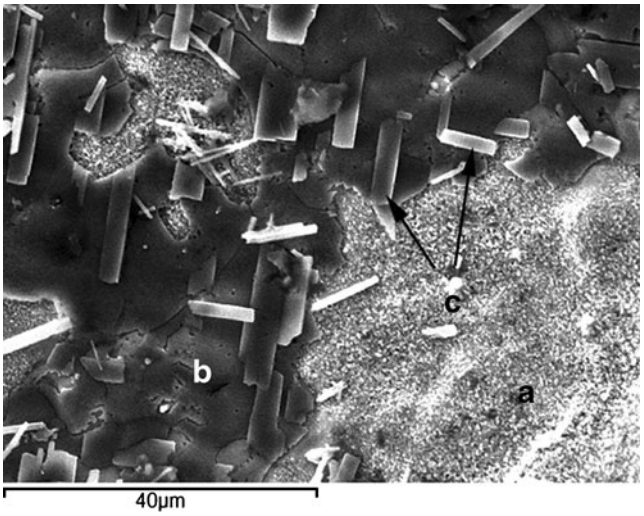

Fig. 8 SEM image of platinum cathode after electrolysis in 85.7 mol% K_2MoO_4–14.3 mol% MoO_3 melt (1,233 K, −0.1 A cm^{-2}, total charge 60 C cm^{-2}) and subsequent washing by diluted HCl and distilled water. Area *a* corresponds to bare platinum, area *b* to molybdenum-rich sublayer, and *c* corresponds to KMo_4O_6 crystals

KMo_4O_6 formed in the course of electrolysis consists of the dark prismatic crystals of typical sizes ranging from 1–3 μm to 600–800 μm. It is worth noting that the crystals are strongly elongated along the crystallographic *c*-axis, as was reported previously [1]. Besides diffusion limitations during the electrolysis, this shape can result from conductivity anisotropy.

Small inclusions are observed at the crystals surfaces (<3 μm, Mo/Pt ratios 1.8–3.2), which can be attributed to Mo–Pt intermetallic compounds. Origin of these inclusions remains unclear. Incomplete oxidation of initially deposited intermetallic compound or parallel reduction of anodically generated platinum oxides can be expected. Besides these inclusions, EDX reveals small amounts of Pt (1.5–4 wt.%), Ti (0.5–1.2 wt.%), and Al (<0.5 wt.%) in various points of the samples.

Pulsed electrodeposition

Pulsed mode can be also applied to change the Mo/MoO_3 ratio in a near-electrode diffusion layer containing initial deposit in contact with the melt of variable composition, and hence to change the crystal size [31]. In this case during the pulse of negative current (−0.1 A cm^{-2}), we expect the metallic molybdenum deposition. After the deposition pulse, the short period of zero current follows, which allows for further oxidation of the deposit and recovery of ions concentrations in diffusion layer. Thus, varying the time ratio of both steps one can influence (to some extent) the ratio of contributions from electrochemical and chemical reactions.

As expected, when shortening the duration of the cathodic pulse we obtained smaller KMo_4O_6 crystals (Fig. 9). Besides, small rounded crystals with slightly higher Mo/K ratio=5±1 appeared.

In contrast to solids obtained under galvanostatic deposition mode, phase composition of the deposits formed under pulse mode is rather complex. Full profile refinement of the XRD patterns was complicated, and quantitative estimation of phase contents was impossible. Complications go from the presence of unidentified admixtures and from peak splitting of both KMo_4O_6 and MoO_2 phases. It is possible that the latter indicates the presence of several phases structurally related to MoO_2 or KMo_4O_6, which are not described in literature. Information concerning major identified phases is summarized in Table 3.

Despite of abovementioned difficulties, XRD phase analysis (Table 3) confirms the increase of the content of more oxidized molybdenum compounds ($K_3Mo_{14}O_{22}$ and MoO_2) with decrease in duty cycle (Fig. 7b). Similar change in deposit phase composition can be achieved under galvanostatic mode either by decreasing the current density or increasing the MoO_3 content (compare Tables 2 and 3). As the time-off increases, one can expect successive oxidation Mo→KMo_4O_6→$K_3Mo_{14}O_{22}$→MoO_2. However, the observed trend for crystals size KMo_4O_6>MoO_2>$K_3Mo_{14}O_{22}$ as well as the principal difference in the $K_3Mo_{14}O_{22}$ crystal shapes do not confirm this hypothesis and indicate the necessity of further detalization of the mechanism in future (i.e., consideration of nucleation kinetics).

Low temperature melts (823–933 K)

The independent verification of proposed EC deposition mechanism was also performed in wider interval of acidity, with involvement of lower temperatures. One can assume that the decrease in temperature should result in (1) cathodic shift of the main reduction process *E′* and (2) the decrease in the rate of subsequent chemical step. Increase in acidity should induce an opposite effect.

Figure 10, curve 1 shows voltammogram of platinum electrode in acidic molybdenum melt (50 mol% MoO_3) at 823 K. No redox processes in the range from −0.925 to −0.3 V are observed under these conditions. The characteristic potential of redox process *E*/*E′* is indeed more negative than those that have been reported above for higher temperatures (Fig. 5b). A huge shift of *E*/*E′* potential (0.766 V per decade) to more positive values was observed with MoO_3 addition. Within the experimental accuracy, the value of this shift is in good agreement with the values found at higher temperatures. There is a small pre-wave at ca. −0.75 V and a distinct reduction wave at −0.835 V in melt with 75 mol% MoO_3. To clarify the nature of this pre-wave, we performed a number of preparative electrodeposition experiments at low current densities, but no solid deposits were obtained. At higher current densities, blue (at 843 K) and a mixture of

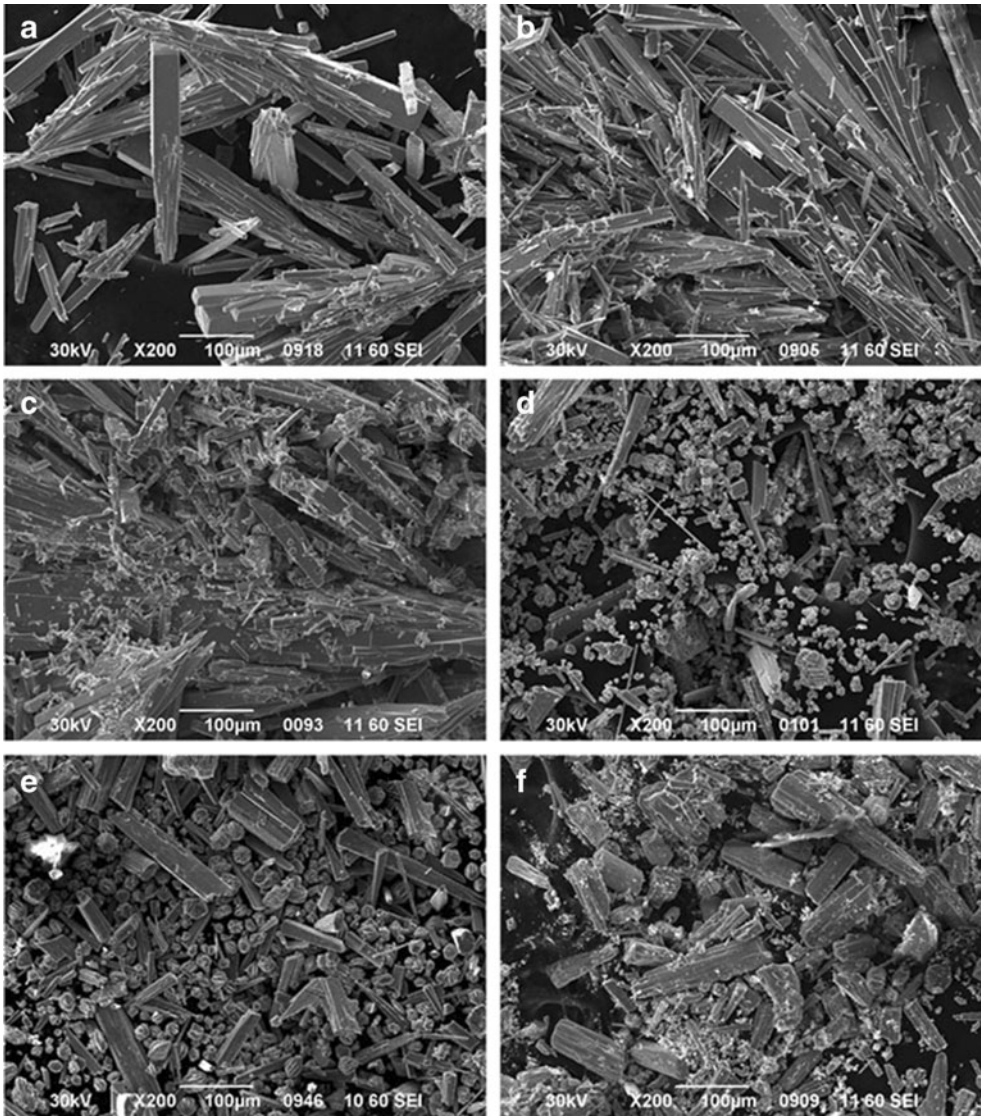

Fig. 9 The SEM images of deposits obtained under galvanostatic (**a**) and pulsed (**b**–**f**) regimes in 85.7 mol% K_2MoO_4–14.3 mol% MoO_3 melt. Q=1,000–1,300 C cm^{-2}, f=3 Hz, T=1,233 K, duty cycles: 66 % (**b**), 60 % (**c**), 55 % (**d**), 50 % (**e**), and 23 % (**f**)

blue and red (at 853 K) bronzes (Table 2) were obtained. Only MoO_2 can be obtained as an electrolysis product at temperatures above 873 K or at lower melt acidity.

As expected from thermodynamic estimates, heating leads to the shift of all reduction peaks toward positive potentials (inset in Fig. 10). However, this shift is too large (65 mV in the region from 853 to 933 K) as compared with the estimated values (23 mV) and cannot be explained in frames of available thermodynamic data. Nevertheless, all observed trends are in good agreement with our predictions. Furthermore, we could not find any peculiarity in redox behavior which could be associated with a narrow temperature range of electrosynthesis of bronzes.

On the other hand, it is well known that typical chemical synthesis of bronzes can be performed by heating of a melt (K_2MoO_4+MoO_2+MoO_3) in evacuated sealed tubes [32, 33] or, alternatively, by temperature gradient flux technique [34–36]. For both routes, the nature of reaction product depends both on the ratio of melt components and on the temperature gradient. Considering these facts, we assume

Table 3 Electrodeposition conditions and main components of deposits obtained under galvanostatic and pulsed regimes in 85.7 mol% K_2MoO_4–14.3 mol% MoO_3 melt

Duty cycle	100 % (galvanostatic)	67 %	60 %	55 %	50 %	23 %
Phase composition	KMo_4O_6	KMo_4O_6 MoO_2	KMo_4O_6 MoO_2	MoO_2 $K_3Mo_{14}O_{22}$ KMo_4O_6	MoO_2 $K_3Mo_{14}O_{22}$ KMo_4O_6	MoO_2

i=−0.1 A cm^{-2}, f=3 Hz, Q=1,030–1,370 C cm^{-2}, T=1,233 K

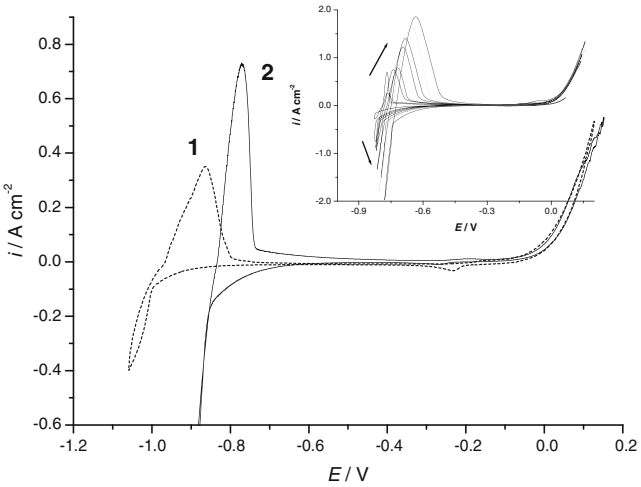

Fig. 10 Cyclic voltammograms of platinum electrode in 50 mol% K_2MoO_4–50 mol% MoO_3 melt at 823 K (*1*) and in 25 mol% K_2MoO_4–75 mol% MoO_3 melt at 843 K (*2*). The *inset* presents cyclic voltammograms of platinum electrode in 75 mol% K_2MoO_4–25 mol% MoO_3 melt at temperatures 833–903 K. Increment 10 K. Scan rate 100 mV s^{-1}

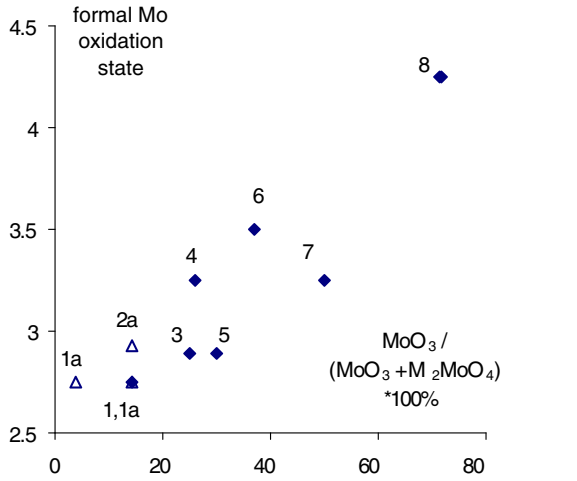

Fig. 11 Dependence of the formal molybdenum oxidation state in reduced molybdenum oxides on MoO_3 content in the melt: KMo_4O_6, [1] (*1*), $K_3Mo_{14}O_{22}$ [2] (*2*), $Nd_4Mo_{18}O_{32}$ [6] (*3*), $LaMo_8O_{14}$ [4] (*4*), $Sm_4Mo_{18}O_{32}$ [6] (*5*), $NdMo_6O_{12}$ [5] (*6*), $LaMo_{7.7}O_{14}$ [4] (*7*), and $La_5Mo_4O_{16}$ [2, 3] (*8*). All the compounds were obtained by fused salt electrolysis in the $M_2MoO_4/MoO_3/Ln_2O_3$ melts at 1,203–1,373 K. MoO_3 content is calculated with respect to M_2MoO_4–MoO_3, i.e., additional rare earth oxide is not taken into account. Index "*a*" refers to compounds obtained in this work

that the bronze formation includes electrochemical reduction of MoO_3 to MoO_2 and subsequent chemical oxidation:

$$3\ K_2MoO_4 + 3\ MoO_2 + 14\ MoO_3 \rightarrow 20\ K_{0.3}MoO_3$$

Discussion

Experimental data on electrochemistry of molybdate melts along with the thermodynamic estimates allowed us to assume the nature of several electrochemical redox-processes and to demonstrate the possibility for parallel chemical oxidation reactions. These data are also helpful to explain some trends for formation of certain electrodeposited solids as affected by current density, melt composition, or duty cycle (under pulsed mode).

Unfortunately, any direct comparison with the previously published electrosynthetic results is complicated due to the evident lack of experimental details. We were able to find only a limited number of consistent data for electrodeposition of cluster molybdenum compounds from melts of different compositions [1–6]. All these compounds were fabricated at similar deposition currents (20–40 mA, electrode areas are unknown) and temperatures (1,203–1,373 K). The comparison of melt composition[6] and molybdenum formal oxidation state in final deposits (Fig. 11) demonstrates the same tendency as described above (compare with Table 2): the increase in MoO_3 content results in formation of more oxidized product. It is quite reasonable to explain this fact by acidity effect on molecular composition of electroactive species in the melts. This assumption should be further verified by careful analysis of liquid melt structure. However, our original data on KMo_4O_6 and $K_3Mo_{14}O_{22}$ electrosynthetic experiments (see points 1a and 2a in Fig. 11) demonstrate that other reasons are also possible, at least in K_2MoO_4–MoO_3 melts. In this case we should not ignore significant contribution of chemical oxidation reactions. Our data on scan rate dependence of Mo oxidation peak, as well as the dependence of the nature of electrolysis product on deposition current density, melt acidity, and duty cycle confirm this hypothesis.

The most interesting feature of cluster molybdenum compounds structure is a short Mo–Mo distance (2.754–2.879 Å for KMo_4O_6 [1]), being comparable to that in Mo metal (2.725 Å).[7] The formation mechanism of these molybdenum clusters is still unclear, but it is known that non-electrochemical synthetic procedure for cluster Mo compounds often involves chemical oxidation of metallic molybdenum [38–40]. Therefore, considering our results, we can assume that these molybdenum clusters can appear after the metallic molybdenum oxidation, but not directly in the course of Mo(VI/IV) reduction.

[6] In order to estimate acidity of these melts and to highlight the contribution of MoO_3 as an oxidizing agent, the MoO_3 content is calculated with respect to M_2MoO_4–MoO_3, i.e., additional basicity going from rare earth oxide is not taken into account.

[7] Calculated using atomic coordinates from [37].

Conclusions

Experimental data on electrochemistry of molybdate melts along with the thermodynamic estimates allowed us to assume the nature of several electrochemical redox processes and to demonstrate that the most pronounced reduction wave in basic melts (≤20 mol% MoO_3) can be attributed to the formation of metallic molybdenum. No redox processes were observed which can be assigned to the direct formation of KMo_4O_6 or $K_3Mo_{14}O_{22}$.

The anomalous scan rate dependence of oxidation peak of metallic molybdenum indicates that the reduction mechanism is complicated by a chemical oxidation step. Taking into account the known procedures of chemical synthesis we assumed that the Mo/MoO_3 ratio in a near-electrode diffusion layer is the key parameter affecting the nature of electrolysis product. Of course this parameter cannot be measured (or adjusted) directly, but it can be varied by changing the electrodeposition conditions. The following trends were observed.

1. Lowering the *deposition current* (i.e., Mo content) results in the increase of KMo_4O_6 content in the deposit.
2. At constant deposition current, the increase in *MoO_3 content* from 3.85 to 50.0 mol% leads to formation of more oxidized products, in a sequence KMo_4O_6…$K_3Mo_{14}O_{22}$…MoO_2.
3. More oxidized molybdenum compounds ($K_3Mo_{14}O_{22}$ and MoO_2 instead of KMo_4O_6) were obtained with decrease of *duty cycle* during the pulsed deposition.

In the melts containing 20–50 mol% MoO_3 at high temperatures, the major electrolysis product is MoO_2. Temperature decrease results in formation of a mixture of blue and red (at 853 K) or blue (at 843 K) bronzes, but there are no peculiarities in electrochemical behavior which could be associated with a narrow temperature range of electrosynthesis. The proposed EC mechanism of bronze formation agrees well with known procedures of chemical synthesis.

We hope that the presented data would be useful for initial choice of melt composition and temperature for electrosyntheses of molybdenum cluster compounds. Further precise electrochemical tuning can be performed by setting an appropriate deposition current (or changing a duty cycle under pulsed mode). According to our experience, cell potential can be a helpful indicator of deposition process despite of its complex nature. Typical electrode potential values for molybdenum-reduced oxides deposition in basic melts is −1.0–−1.1 V, which corresponds to molybdenum deposition.

The values of current density reported above are operative for the small-scale laboratory cell in the absence of forced convection. For larger-scale electrolysis inducing the specific hydrodynamic phenomena, as well as for the cells with melt stirring higher current densities are required, which should be specified for any unusual bath configuration. However, the effects of key factors listed above are valid independently of these conditions affecting the specific features of mass transport.

Acknowledgments Authors are grateful to Dr. Anastasiya M. Alekseeva for her help with XRD data collection and valuable comments concerning phase analysis and to Dr. Leonid A. Solovyov for his help in data treatment using DDM software.

References

1. Ramanujachary KV, Greenblatt M, Jones EB, McCarroll WH (1993) J Solid State Chem 102:69–78
2. Ledesert M, Labbe P, McCarroll WH, Leligny H, Raveau B (1993) J Solid State Chem 105:143–150
3. Ramanujachary KV, Greenblatt M, McCarroll WH, Goodenough JB (1993) Mat Res Bull 28:1257–1267
4. Ramanujachary KV, Jones EB, Greenblatt M (1995) J Solid State Chem 117:261–268
5. Tortelier J, McCarroll WH, Gougeon P (1998) J Solid State Chem 136:87–92
6. Lofland SE, Tyagi S, Hettinger JD, McCarroll WH, Ramanujachary KV, Gall P, Gougeon P (2007) Materials Res Bull 42:1230–1241
7. Lommel B (1988) Kristallzüchtung und Charakterisierung von blauen Bronzen, Diploma thesis, Johann-Wolfgang-Goethe-Universität, Frankfurt
8. Wold A, Kunnmann W, Arnott RJ, Ferretti A (1964) Inorganic Chem 3:545–547
9. Ghedira M, Chenavas J, Marezio M (1985) J Solid State Chem 57:300–313
10. Vincent H, Ghedira M, Marcus J, Mercier J, Schlenker C (1983) J Solid State Chem 47:113–121
11. Drobasheva TI, Zueva VP, Spitsyn VI (1980) Zhurnal neorg khimii 25:1694–1697
12. Ravindran NK, Wang E, Greenblatt M (1984) J Solid State Chem 55:193–199
13. Buder R, Devenyi J, Dumas J, Marcus J, Mercier J, Schlenker C (1982) J Physique—Lettres 43:L-59–L-65
14. Strobel P, Greenblatt M (1981) J Solid State Chem 36:331–338
15. Stephenson NC, Wadsley AD (1965) Acta Crystallogr 19:241–247
16. Kalev KA, Baraboshkin AN, Zlokazov VA (1979) Tr Inst Elektrokhim Ural Nauchn Tsentr Akad Nauk SSSR 28:89
17. Malyshev VV, Finadorin AE, Shapoval VI (1997) Ukr Khim Zh (Russ Ed) 63:10–15
18. Shapoval VI, Baraboshkin AN, Kushkhov KB, Malyshev VV (1987) Sov Electrochem 23:885–889
19. Baraboshkin AN, Shunailov AF, Martynov VA (1970) In Proceedings of Institute of Electrochemistry of Ural Division of Academy of Sciences of the USSR, 15:67–69
20. ICDD, PDF2. http://www.icdd.com/products/pdf2.htm, 2012
21. Inorganic Crystal Structure Database (ICSD), Fachinformationzentrum, Karlsruhe, 2005.
22. Solovyov LA (2004) J Appl Cryst 37:743–749
23. HSC Chemistry 5.11 Database (2002) Outokumpu Research Oy. Pori. Finland
24. Lin RY, Elliott JF (2001) J Alloy Comp 321:261–266
25. Benarchid MY, David N, Fiorani JM, Vilasi M, Benlaharche T (2009) J Chem Thermodynamics 41:383–385
26. Jacob KT, Abraham KP, Ramachandran S (1990) Metallurgical Mater Trans B 21:521–527

27. Brewer L, Lamoreaux H, Ferro R, Marazza R (1980) J Phase Equilibria 1:89–92
28. Topor DC, Selman JR (1993) J Electrochem Soc 140:352–361
29. McCarroll WH, Ramanujachary KV, Greenblatt M, Marsh RE (1995) J Solid State Chem 117:217–218
30. Schimek GL, Chen SC, McCarley R (1995) Inorg Chem 34:613
31. Sandmann G, Dietz H, Plieth W (2000) J Electroanal Chem 491:78–96
32. Ganne M, Boumaza A, Dion M, Dumas J (1985) Mater Res Bull 20:1297–1308
33. Aichele T (2007) Cryst Res Technol 42:419–423
34. McCarroll WH, Greenblatt M (1984) J Solid State Chem 54:282–290
35. Ramanujachary KV, Greenblatt M, McCarroll WH (1984) J Cryst Growth 70:476–483
36. Collins BT, Ramanujachary KV, Greenblatt M, Waszczak JV (1985) Solid State Commun 56:1023–1028
37. Swanson HE, Tatge E (1953) National Bureau of Standards (U.S.). Circular 539:1–95
38. Hoffman R, Hoppe R (1990) J Less-Common Metals 161:279–293
39. Li KH, McCarley RE, Kim S, Jacobson RA (1986) J Solid State Chem 64:347–358
40. Gall P, Gougeon P (2006) Acta Cryst E E62:i155–i157